Deformable Registration Combined with 3D SIFT Matching and Moving Least Squares

Zisheng Li and Tsuneya Kurihara

Central Research Laboratory, Hitachi, Ltd., 1-280 Higashi-Koigakubo, Kokubunji-shi, Tokyo 185-8601 Japan
{zisheng.li.fj, tsuneya.kurihara.vn}@hitachi.com

Abstract. Free-form deformation (FFD) is widely used in deformable image registration. FFD uses a regular grid of control points to generate image deformation. Accurate optimization of the control-point displacement relies on an appropriate initial-deformation of the regular grid. In this work, a hybrid registration of landmark-based and free-form deformation is proposed and applied to lung CT images. Corresponding landmark-pairs are detected and matched by 3D SIFT (scale-invariant feature transform). Using the landmark pairs, Moving Least Squares (MLS) is applied for deforming the regular grid. Utilizing the deformed control-point grid, a landmark-constrained FFD registration obtains a final registration result. Since this landmark-based deformation approach can obtain smooth and local deformation of the control-point grid, the proposed registration can directly start with the initialized control-point grid, without the need for any coarse-to-fine processing. It was experimentally demonstrated that the proposed hybrid-registration method outperforms conventioal FFD registration in terms of efficiency and accuracy.

Keywords: deformable registration, landmark-based deformation, 3D SIFT, 3D MLS

1 Introduction

Image registration is one of the most fundamental research areas in medical-image processing. It aims to find a spatial transformation that maps points from one image, the *moving* image, to the corresponding points in another image, the *fixed* image. Moreover, it is categorized as rigid or non-rigid (deformable). Utilizing translations and rotations only, rigid registration maps a moving image to a fixed image, while deformable registration allows local deformation of the images. Although rigid registration is sufficient in certain circumstances, deformable registration (which provides accurate and local deformation) is required in more and more clinical cases, since tissues and organs of the human body deform, shrink, and grow over time.

Deformable registration can be classified as feature-based methods, intensity-based methods, or a combination of the two. Feature-based methods extract and match corresponding landmarks and estimate a deformation field on the basis of the landmark

locations [1-2]. However, such methods need to interpolate the sparse set of landmarks to obtain correspondences from non-feature locations. They therefore require automatic and high-accuracy matching of a large number of landmarks, which is not an easy task. Intensity-based methods use image intensity to derive the deformation field. Free-form-deformation (FFD) registration [3] is a widely used intensity-based method. It places a regular grid of control points on a moving image and obtains the deformation field from the displacement of the control points and B-spline functions. The FFD method therefore tends to incur a large computational cost, and it often requires an appropriate starting point (i.e., initialization) for optimization of the deformation field, since the number of control points is typically large [4]. To provide an appropriate initialization of the control-point grid to guide the deformable registration, methods combining landmark-based registration and FFD registration have been proposed [5-6]. In [5], corresponding landmarks in coarse scale were located and used for determining a rigid registration as a starting point of multi-scale deformable registration. Such a rigid or affine registration, however, can only handle bony structures; it cannot provide an appropriate initialization for local deformation of human organs. In [6], to handle medical images with high resolution and large size, a registration framework consisting of two separate deformable-registration steps was proposed. A landmark-constrained deformable registration was proposed as an initialization step for the other dense deformable registration. However, the landmark-constrained registration described in [6] used a rigid registration as a starting point, possibly leading to misalignment.

In this work, a hybrid registration of landmark-based and free-form deformation is proposed. Aiming to obtain an appropriate control-grid initialization that can handle local deformation of human organs, a landmark-based-deformation approach is developed. For detecting and matching corresponding landmark pairs, a robust feature-point matching approach that widely used in computer vision literatures is utilized. Using the point-matching results, instead of a rigid/affine registration, smooth and local deformation are applied to the control-point grid. As a result, an appropriate starting point of FFD registration can be obtained. Using the initialized control grid, a landmark-constrained B-spline registration for obtaining a final registration result, without any coarse-to-fine processing, is also developed.

2 Method

This work aims to improve the efficiency and accuracy of deformable image registration by providing an appropriate starting point of the registration. It focuses on the initialization of the control-point grid. This initialization should be able to not only compensate global artifacts but also handle local deformation. Therefore, instead of the widely used rigid registration, landmark-based deformation of the control-point grid, for improving the initialization of FFD registration, is proposed. As shown in Fig. 1, the overall method (i.e., hybrid registration) consists of three steps: corresponding-landmark detection and matching, landmark-based deformation of a regular control-point grid, and landmark-constrained B-spline registration. Corresponding

landmark pairs are detected and matched by 3D SIFT (scale-invariant feature transform) [7]. Using the landmark pairs, Moving Least Squares (MLS) [8] is applied for deforming the control-point grid of B-spline registration. Using the deformed control-point grid as a starting point, a landmark-constrained B-spline registration (for obtaining the final registration result) is developed. SIFT can detect and match corresponding feature points in different scales and rotations, and MLS can obtain smooth and local deformation of the control-point grid; therefore, the landmark-constrained registration can start directly with the initialized control-point grid, without the need for any coarse-to-fine processing.

2.1 3D Landmark Detection and Matching

For obtaining corresponding landmarks from pulmonary images, segmentation of blood vessels or bronchial airways [22-23], 3D operators for cornerness measure [24], and image-block matching techniques [25] are commonly utilized. However, approaches mentioned above are difficult to deal with changes of scaling and rotation robustly. On the other hand, in 2D image matching, SIFT is an effective approach and has been widely used since its original introduction by Lowe [21]. It focuses on extracting salient interest points that can be represented by stable feature descriptors. Such descriptors are invariant to changes of scaling, translation, and orientation. In the field of medical-image analysis, Cheung and Hamarneh extended the 2D SIFT approach to a multi-dimensional one [7]. Applications of an extended 3D SIFT to

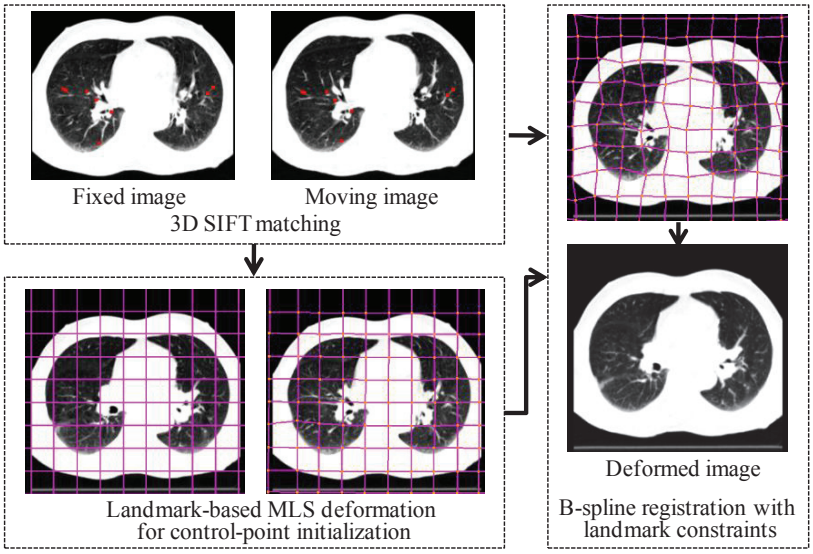

Fig. 1. Framework of the proposed method.

medical-image matching [18-19] and panoramic medical stitching [20] were also proposed. Accordingly, in the present study, the 3D SIFT method [7] is used for detecting and matching corresponding landmarks.

Detection of 3D Keypoints

SIFT feature points can be detected by using difference-of-Gaussian (DoG) images [21]. For a medical image, which is usually a 3D volume, DoG images can be generated as follows [7]:

$$D(x, y, z, k^i\sigma) = L(x, y, z, k^{i+1}\sigma) - L(x, y, z, k^i\sigma), \quad (1)$$

where k is a constant multiplicative factor. $L(x, y, z, \sigma)$ is obtained by smoothing original image $I(x, y, z)$ with variable-scale Gaussian filter $G(x, y, z, \sigma)$:

$$\begin{aligned} L(x, y, z, \sigma) &= G(x, y, z, \sigma) * I(x, y, z) \\ &= \frac{1}{(\sqrt{2\pi}\sigma)^3} e^{-(x^2+y^2+z^2)/2\sigma^2} * I(x, y, z). \end{aligned} \quad (2)$$

From such DoG images, local extrema can be detected at the pyramid level of σ. For voxel v in a DoG image with scale σ, the intensity of v is compared with those of its 80 neighboring voxels (26 neighboring points at σ, 27 counterparts at scale $k^1\sigma$, and 27 counterparts at $k^{-1}\sigma$). The voxel with the most or least extreme value of intensity is considered as a feature point. In this work, multi-scale searching parameters are set as $k = 2.0^{1/3}$ and $\sigma = \{1.00, 1.26, 1.58, 2.00, 2.52, 3.17, 4.00\}$.

3D Keypoint Orientation

Each detected keypoint as explained in the above section is assigned with a dominant orientation $(\theta, \emptyset)$ according to local image properties. The gradient orientation in 3D space is represented by two angles: azimuth θ and elevation $\emptyset$. The 3D gradient at location (x, y, z) can be denoted as

$$\begin{aligned} L_x &= L(x+1, y, z, \sigma) - L(x-1, y, z, \sigma), \\ L_y &= L(x, y+1, z, \sigma) - L(x, y-1, z, \sigma), \\ L_z &= L(x, y, z+1, \sigma) - L(x, y, z-1, \sigma), \end{aligned} \quad (3)$$

and the dominant orientation is defined as

$$\begin{aligned} \theta &= \arctan\left(\frac{L_y/\Delta_y}{L_x/\Delta_x}\right), \\ \emptyset &= \arctan\left(\frac{L_z/\Delta_z}{\sqrt{(L_x/\Delta_x)^2 + (L_y/\Delta_y)^2}}\right), \end{aligned} \quad (4)$$

where $\Delta_x, \Delta_y, \Delta_z$ are voxel sizes. A 2D histogram is produced by grouping gradients around a keypoint in bins that divide azimuth and elevation into sections at 45° intervals. Peaks in this 2D histogram exceeding 80% of the largest peak are used to determine the dominant orientation.

3D Feature Description and Matching

Once the orientation of a keypoint is determined, $4 \times 4 \times 4$ sub-regions surrounding the keypoint are sampled and rotated according to the orientation. For each sub-region, magnitude of the gradient, weighted by a Gaussian window centered at the keypoint, is added to the corresponding bin, where eight bins for azimuth ($-\pi \sim \pi$) and four bins for elevation ($-\pi/2 \sim \pi/2$). Finally, the feature vector is of $4 \times 4 \times 4 \times 8 \times 4 = 2{,}048$ dimensions.

The constructed SIFT features of a keypoint are converted to a single vector, and distances between a feature vector in one image is compared with every feature vector of the second image. A match is distinct when the ratio of the nearest-neighbor distance to the second-nearest one is below 60%, which is adopted in this work.

Outlier Removal

To improve the accuracy and robustness of landmark matching, outliers in the SIFT matching are removed by using a RANSAC algorithm [9] as follows:

Step 1:

Randomly select 3 landmark pairs from the obtained landmarks $\boldsymbol{p}_i$ and $\boldsymbol{q}_i$, and estimate a rigid transformation $\mathrm{T_R}(\boldsymbol{x})$ with the selected landmark pairs, where $\boldsymbol{x}$ represents a certain landmark among $\boldsymbol{p}_i$.

Step 2:

Apply $\mathrm{T_R}(\boldsymbol{x})$ to all of landmarks $\boldsymbol{p}_i$, compute the distance between the transformed landmarks and their corresponding ones: $d_i^2 = \|\boldsymbol{q}_i - \mathrm{T_R}(\boldsymbol{p}_i)\|^2$.

Step 3:

When the above distance is smaller than a threshold ${d_{\mathrm{th}}}^2$, such landmarks are considered as inliers. This threshold is computed as ${d_{\mathrm{th}}}^2 = \mathrm{F}_m^{-1}(\alpha_\mathrm{r})\sigma_\mathrm{r}^2$, where $\mathrm{F}_m^{-1}(\alpha_\mathrm{r})$ represents the threshold value of a Chi-square distribution with degrees of freedom m, α_r is the proportion of inliers that determined by the threshold, σ_r is the standard deviation of d_i. In this work, $m = 3$ and $\alpha_\mathrm{r} = 0.9$ are determined, and the resulting threshold value is $\mathrm{F}_3^{-1}(0.9) = 6.251$.

Step 4:

Estimate the iteration number by

$$N_\mathrm{r} = \frac{\log(1-\xi)}{\log(1-(1-\epsilon)^2)}, \tag{5}$$

where ϵ is the current proportion of outliers. Equation (5) ensures that within N_r trials, the probability to obtain a sample set with no outliers is ξ, which is set as 0.99.

Step 5:

Repeat steps 1-4 until the iteration number exceeds N_r.

Step 6:
Select the obtained inliers with the largest number within N_{r} trials.

2.2 Control-point Grid Deformation

To obtain an appropriate initialization of an FFD registration, the regular control-point grid is deformed by a landmark-based deformation approach. Thin-plate splines (TPS) [1] is a widely used non-rigid transformation model that utilizes sparse corresponding landmarks as control points of the deformation. However, as for TPS, each landmark has a global effect on the transformation. As a result, the accuracy of the deformation is easily affected by outliers. On the other hand, MLS [8] was proposed for interactive animation in computer graphics. This approach is capable of producing local deformation with a small number of corresponding points. In other words, it can overcome the limitations of the landmarks' global effect in the case of TPS. In recent years, therefore, MLS attracts more and more attention in regard to landmark-based registration. In [2] and [10], 3D corresponding landmarks were matched by weighted cross correlation and user annotation, respectively, and deformation of each voxel was obtained by MLS. In [11], the original 2D SIFT proposed by Lowe [21] was applied to detect and match corresponding landmarks for 2D brain images, and the original 2D MLS was utilized for obtaining deformation of each pixel. However, to find transformations of every pixel/voxel in an image is a time-consuming procedure, which lowers the efficiency of registration.

In this work, landmark-based deformation is not applied for finding transformations of every image voxel in a registration; instead, it is utilized for obtaining deformation of the regular control-point grid, i.e., an initialization of an FFD registration. Since MLS can avoid global effects of each landmark, 3D MLS is adopted as the landmark-based deformation approach in the proposed registration framework.

In MLS, aiming to find the best rigid transformation $l_{\boldsymbol{v}}(\boldsymbol{x})$ of a control point $\boldsymbol{x} = \boldsymbol{v}$ on the fixed image, the following equation is minimized:

$$\begin{aligned} &\arg\min_{l_v} \sum_{i=1}^{N} w_i |l_{\boldsymbol{v}}(\boldsymbol{p}_i) - \boldsymbol{q}_i|^2 , \\ &w_i = 1/|\boldsymbol{p}_i - \boldsymbol{v}|^{2\alpha} , \end{aligned} \tag{6}$$

where $\boldsymbol{p}_i$ and $\boldsymbol{q}_i$ are corresponding landmark pairs obtained by SIFT matching; N is the landmark number; weights w_i have the form of least squares while being dependent on distances between control point $\boldsymbol{v}$ and landmark $\boldsymbol{p}_i$; α is set as 1.0 experimentally. As a result, a unique transformation $l_{\boldsymbol{v}}(\boldsymbol{v})$ can be obtained for each control point $\boldsymbol{v}$; and such transformations can provide smooth and local deformation of the control points, on the basis of the corresponding landmark pairs.

Since the control-point displacements obtained by MLS are reliable, the initial B-spline curves used in the FFD registration are constructed so that they pass through the obtained control points. Definition points $\boldsymbol{Q}_i$ $(i = 0,1,2,\cdots,n)$ of such B-spline curves can be calculated by the following equation:

$$\frac{1}{6}\boldsymbol{Q}_{i-1}+\frac{2}{3}\boldsymbol{Q}_i+\frac{1}{6}\boldsymbol{Q}_{i+1}=\boldsymbol{P}_i \ \ (i=1,2,\cdots,n-1), \tag{7}$$

where $\boldsymbol{P}_i$ are the control points obtained by MLS. In equation (7), since there are n equations and n+2 unknowns, to find a set of unique solutions, two boundary conditions are required. In this work, the boundary conditions are set as $\boldsymbol{Q}_0=\boldsymbol{Q}_1$ and $\boldsymbol{Q}_n=\boldsymbol{Q}_{n-1}$; i.e., the curves are opened, and curvatures of two ends of such curves are 0. Utilizing cubic B-spline interpolation techniques in [26], $\boldsymbol{Q}_i$ can be solved efficiently.

2.3 Landmark-constrained FFD Registration

The deformed control-point grid is used as a starting point of an FFD registration. To obtain faster and better convergence of optimization in the registration procedure, a landmark-constrained approach [6] is adopted. Geometric information of the landmark pairs is incorporated into cost function S in the optimization process. The resulting S is formulated as

$$\mathrm{S}\big(\boldsymbol{R},\boldsymbol{F},\boldsymbol{U}(\boldsymbol{x})\big)=-\mathrm{MI}\big(\boldsymbol{R},\boldsymbol{F},\boldsymbol{U}(\boldsymbol{x})\big)+\lambda\mathrm{C}\big(\boldsymbol{U}(\boldsymbol{x})\big)+\mu\sum_{\boldsymbol{x}\in\boldsymbol{P}}\|\boldsymbol{U}(\boldsymbol{x})-\boldsymbol{V}(\boldsymbol{x})\|^2, \tag{8}$$

where $\boldsymbol{R}$ and $\boldsymbol{F}$ are the fixed and moving images; $\boldsymbol{U}(\boldsymbol{x})$ is a displacement field of the moving image, obtained by B-spline functions; MI is mutual information [12] of $\boldsymbol{R}$ and the transformed $\boldsymbol{F}$; C is a bending-energy regularization term [3] calculated from $\boldsymbol{U}(\boldsymbol{x})$ to enforce smooth deformation of $\boldsymbol{F}$; $\boldsymbol{P}$ indicates the corresponding pairs; $\boldsymbol{V}(\boldsymbol{x})$ denotes displacements at these points given by the landmark matching results; and λ and μ are weighting factors determined experimentally. In this manner, landmark-matching results are also incorporated into the cost function of the deformable registration, aiming to make the optimization process converge in an accurate and fast way. In this work, the L-BFGS (limited-memory Broyden–Fletcher–Goldfarb–Shanno) algorithm [13] is applied to the optimization procedure.

3 Experimental Results

3.1 Clinical Data for Evaluation

Two sets of pulmonary CT images were used to evaluate the proposed method. The first dataset was composed of lung CT images from cases 1-5 of a DIR-lab dataset [2]. The provided images were originally cropped to include the entire rib cage and sub-sampled to 256×256 voxels in the axial plane. The image resolution was 0.97 to 1.16 mm in the axial plane, and 2.5 mm in the z-direction. The second dataset, also from the DIR-lab dataset, was composed of lung CT images from cases 6-10 [14]. These images were not originally sub-sampled or processed in any way. The image

resolution was 0.97 mm, with 512×512 voxels in the axial plane and 2.5 mm in the *z*-direction. All the image pairs from the DIR-lab were measured at the extreme inhale and exhale phases, respectively.

As ground-truth data for accuracy evaluation, corresponding landmarks were manually annotated in the fixed and moving images by DIR-lab, and 300 landmarks per image were made publicly available [2, 14].

3.2 Evaluation Results

Euclidean distances between the manually annotated landmarks and the transformed correspondences in the moving images were used to calculate the registration spatial error. The mean and standard deviation (SD) values of the Euclidean distances were obtained from the two datasets, respectively.

To compare the performance of the proposed method with a state-of-the-art FFD-

Table 1. Parameters and strategies of registration.

	Control-grid initialization	Coarse-to-fine level	Sample number	Optimization	Maximum iteration
Proposed	Landmark-based deformation	1	30,000-180,000 (Sample proportion: 0.5%)	L-BFGS*	50
FFD	Affine transformation	4	2,000-3,000	ASGD**	4,000-8,000

*L-BFGS [13]: limited-memory Broyden–Fletcher–Goldfarb–Shanno algorithm

**ASGD [15]: adaptive stochastic gradient descent algorithm

Table 2. Running time and landmark number of SIFT matching.

Dataset	DIR-lab dataset Cases 1-5	DIR-lab dataset Cases 6-10
Running time [s]	15	48
Landmark number (SD)	1,028 (176)	1,248 (185)

Table 3. Evaluation results of DIR-lab dataset (cases 1-5).

	MLS + interpolation	Proposed	FFD
Coarsest/finest grid size [mm]	-/32	-/32	128/16
RMS error (SD) [mm]	2.35 (0.58)	1.45 (0.35)	2.03 (0.48)
Running time [s]	16	23	462

Table 4. Evaluation results of DIR-lab dataset (cases 6-10).

	MLS + interpolation	Proposed	FFD
Coarsest/finest grid size [mm]	-/32	-/32	128/16
RMS error (SD) [mm]	4.16 (1.08)	2.54 (0.64)	3.99 (1.29)
Running time [s]	51	92	1366

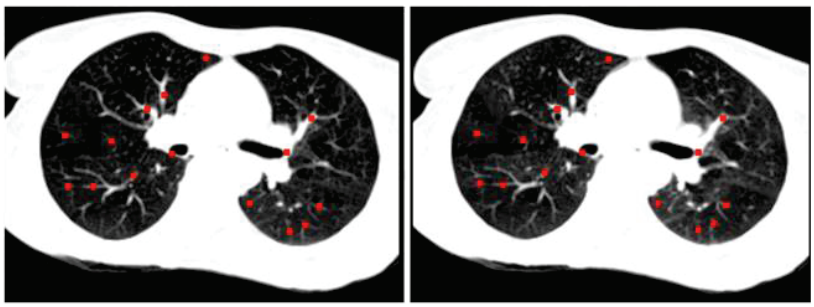

Fig. 2. Examples of SIFT matching results.

based registration method, the deformable registration module of the Elastix toolkit [15] was evaluated. In [15], the control-point grid was initialized by using an affine registration of the fixed and moving images. Moreover, in [15], a multi-level coarse-to-fine scheme is applied to handle large motions. On the other hand, the proposed method applies 3D SIFT matching and MLS to initialize the control-point grid, and it directly runs the landmark-constrained registration at the finest resolution level. Parameters and registration strategies of the two methods are listed in Table 1. "Sample number" denotes numbers of sample points for computation of image similarity metric. In this work, selection of such sample points is based on a series of Halton sequences [16-17]; while that of the FFD registration in [15] is based on random coordinates.

In addition, to validate the effectiveness of the proposed landmark-based deformation, a registered image is generated by directly interpolating the initialized grid instead of performing the landmark-constrained optimization procedure. In this way, the accuracy of the landmark-based deformation was also evaluated by using the same datasets. Lung masks were not used in the three above-mentioned methods in these experiments.

The running time and final landmark number (mean and SD values) of the SIFT matching and RANSAC procedures are listed in Table 2, for the two datasets, respectively. A CT value threshold, [250-800], is experimentally set, and voxels that have a CT value within the threshold range are considered as being inside the lung. The SIFT matching is performed in such regions. Examples of SIFT matching results for case 1 of the DIR-lab dataset are shown in Figure 2. Red points shown in the figure represent corresponding landmarks.

The results of an evaluation using the two datasets for the three above-described approaches are listed in Tables 3 and 4. For the second dataset, cases 6-10 of the DIR-lab dataset, since the image size is large and the rib cage of the patient's body is not cropped out, the parameters of the FFD registration need to be modified. Number of sample points and maximum iterations of optimization are increased to 3,000 and 8,000, respectively. The proposed method, in contrast, is able to deal with the two datasets with the same parameter set. These parameters were tuned on two image-pairs of cases 1-5 of the DIR-lab dataset. Moreover, it should be noted that the run-

ning times of MLS deformation and the proposed method include that for SIFT matching processing for all of the evaluation results listed in Tables 3 and 4.

It is clear that the proposed method outperforms the conventional FFD deformable registration to a large extent, both in terms of efficiency and accuracy. Thanks to the accuracy and robustness of SIFT matching, the MLS deformation can provide good performance of registration without need for any coarse-to-fine procedures. Consequently, the landmark-based deformation provides an appropriate starting point for FFD registration. Furthermore, landmark-constrained optimization contributes to fast convergence of the proposed registration. Overall, the proposed method outperforms the conventional FFD registration [15] by achieving 30% better accuracy and more than 15 times higher processing speed.

4 Conclusion and Future work

A hybrid registration method of landmark-based deformation and FFD registration is proposed and applied to the registration of lung CT images. Aiming to obtain an appropriate control-grid initialization that can handle local deformation of human lungs, a landmark-based deformation approach is proposed. Using an initialized control grid as a starting point, landmark-constrained FFD registration, to obtain a final registration result without need for any coarse-to-fine processing, is developed.

To detect and match corresponding landmark pairs, 3D SIFT matching is developed. Using the obtained landmark pairs, 3D MLS deformation is applied for deforming the regular control-point grid of an FFD registration. As a result, smooth and local deformation of the control-point grid can be obtained as an appropriate starting point for deformable registration. Furthermore, a landmark-constrained approach for obtaining faster and better convergence of the registration is also developed. Evaluation experiments on lung CT images show that the proposed method, with a fixed parameter set, is able to perform an efficient and accurate registration on actual clinical data without any coarse-to-fine processing. Compared with a conventional FFD registration, the proposed method achieves 30% better accuracy and more than 15 times higher processing speed.

Since the running time of landmark matching occupies a large proportion of that of the proposed registration approach, the landmark-matching algorithm needs to be speeded up. In addition, the robustness and accuracy of landmark matching needs to be validated by using images with larger deformation and higher noise level. Furthermore, the proposed method should be evaluated in terms of inter-patient registration tasks.

Acknowledgement

We would like to thank the DIR-lab, the University of Texas M. D. Anderson Cancer Center, for providing the clinical data and the annotated landmarks.

References

1. Rohr, K., et al.: Landmark-based elastic registration using approximating thin-plate splines. IEEE Trans. Medical Imaging, 20, 6, 526--534 (2001)
2. Castillo, R., et al.: A framework for evaluation of deformable image registration spatial accuracy using large landmark point sets. Phys. Med. Biol., 54, 1849--1870 (2009)
3. Rueckert, D., et al.: Nonrigid registration using free-form deformations: Application to breast MR images. IEEE Trans. Medical Imaging, 18, 8, 712--721 (1999)
4. Sotiras, A., Davatazikos, C., and Paragios, N.: Deformable medical image registration: a survey. HAL: hal-00684715, version 3, Research report, no. 7919 (2012)
5. Paquin, D., Levy, D., and Xing, L.: Hybrid multiscale landmark and deformable image registration. Mathematical Biosciences and Engineering, 4, 4, 711--737 (2007)
6. Han, X.: Feature-constrained nonlinear registration of lung CT images. In: MICCAI EMPIRE10 Challenge, 2010, pp. 63--72 (2010)
7. Cheung, W. and Hamarneh, G.: N-SIFT: n-dimensional scale invariant feature transform. IEEE Trans. Image Processing, 18, 9, 2012--2021 (2009)
8. Schaefer, S., McPhail, T., Warren, J.: Image deformation using Moving Least Squares. ACM TOG, 25, 3, 533--540 (2006)
9. Fischler, M. and Bolles, R.: Random sample consensus: a paradigm for model fitting with applications to image analysis and automated cartography. Communications of the ACM, 24, 6, 381--395 (1981)
10. Menon, H. P. and Narayanankutty, K. A.: Applicability of non-rigid medical image registration using Moving Least Squares. International Journal of Computer Applications, 1, 6, 79--86 (2010)
11. Arun, K. S. and Sarath, K. S.: An automatic feature based registration algorithm for medical images. In: Proceeding of ARTCom 2010. pp. 174--177 (2010)
12. Pluim, J. P. W., Maintz, J. B. A., and Viergever, M. A.: Mutual-information-based registration of medical images: a survey. IEEE Trans. Medical Imaging, 22, 8, 986--1004 (2003)
13. Nocedal, J.: Updating quasi-Newton matrices with limited storage. Mathematics of Computation, 35, 151, 773--782 (1980)
14. Castillo, E., et al.: Four-dimensional deformable image registration using trajectory modeling. Phys. Med. Biol., 55, 305--327 (2010)
15. Klein, S., et al.: Elastix: A toolbox for intensity-based medical image registration. IEEE Trans. Med. Imaging, 29, 1, 196--205 (2010)
16. Thevenaz, P., Bierlaire, M., and Unser, M.: Halton sampling for image registration based on mutual information. Journal of STSIP, 7, 2, 141--171 (2008)
17. Li, Z., Kurihara, T., and Matsuzaki, K.: Efficient Rigid Registration for Medical Images Based on Small Sample Set. IEICE Technical Report, MI, 111, 199, 1--6 (2011)
18. Allaire, S., et al.: Full orientation invariance and improved feature selectivity of 3D SIFT with application to medical image analysis. In: Proceeding of CVPRW 2008. pp. 1--8 (2008)
19. Li, Z., et al.: Evaluation of medical image registration by using 3D SIFT and phase-only correlation. Abdominal Imaging, Computational and Clinical Applications, 255--264 (2012)
20. Ni, D., et al.: Volumetric ultrasound panorama based on 3D SIFT. In: Proceeding of MICCAI 2008. vol. 5242, pp. 52--60 (2008)
21. Lowe, D. G.: Distinctive image features from scale-invariant keypoints. International Journal of Computer Vision, 60, 2, 91--110 (2004)

22. Hilsmann, A., et al.: Deformable 4DCT lung registration with vessel bifurcations. In: CARS 2007, (2007)
23. Huang, Y., et al.: Automatic landmark detection and nonrigid registration of intra-subject lung CT images. In: Intl. Conf. Inf. Sci. Eng., IEEE Computer Society, pp. 3605--3608 (2009)
24. Hartkens, T., Rohr, K., and Stiehl, H.: Evaluation of 3D operators for the detection of anatomical point landmarks in MR and CT images. Comput. Vision Imag. Under., 86, 118--136 (2002)
25. Miyazawa K., et al.: A Novel approach for volume registration using 3D Phase-Only Correlation. In: Radiological Society of North America (RSNA) 2009, pp. 1070 (2009)
26. Unser M., Aldroubi A., and Eden M.: Fast B-spline transforms for continuous image representation and interpolation. IEEE Trans. Pattern Analysis and Machine Intelligence, 13, 3, 277--285 (1991)